© 2023. Published by The Company of Biologists Ltd | Journal of Cell Science (2023) 136, jcs260279. doi:10.1242/jcs.260279

RESEARCH ARTICLE

Mitochondrial respiration promotes Cdc37-dependent stability of the Cdk1 homolog Cdc28

Ana Cláudia Leite[1,2,3,*], Telma S. Martins[1,2,3,*], Rute R. Cesário[1,2], Vitor Teixeira[1,2], Vítor Costa[1,2,3] and Clara Pereira[1,2,‡]

ABSTRACT

Cdc28, the homolog of mammalian Cdk1, is a conserved key regulatory kinase for all major cell cycle transitions in yeast. We have found that defects in mitochondrial respiration (including deletion of *ATP2*, an ATP synthase subunit) inhibit growth of cells carrying a degron allele of Cdc28 (*cdc28td*) or Cdc28 temperature-sensitive mutations (*cdc28-1* and *cdc28-1N*) at semi-permissive temperatures. Loss of cell proliferation in the *atp2Δcdc28td* double mutant is associated with aggravated cell cycle arrest and mitochondrial dysfunction, including mitochondrial hyperpolarization and fragmentation. Unexpectedly, in mutants defective in mitochondrial respiration, steady-state protein levels of mutant *cdc28* are strongly reduced, accounting for the aggravated growth defects. Stability of Cdc28 is promoted by the Hsp90–Cdc37 chaperone complex. Our results show that *atp2Δcdc28td* double-mutant cells, but not single mutants, are sensitive to chemical inhibition of the Hsp90–Cdc37 complex, and exhibit reduced levels of additional Hsp90–Cdc37 client kinases, suggesting an inhibition of this complex. In agreement, overexpression of *CDC37* improved *atp2Δcdc28td* cell growth and Cdc28 levels. Overall, our study shows that simultaneous disturbance of mitochondrial respiration and Cdc28 activity reduces the capacity of Cdc37 to chaperone client kinases, leading to growth arrest.

KEY WORDS: Mitochondria, Cell cycle, Signaling, Yeast, Chaperone

INTRODUCTION

The eukaryotic cell cycle is controlled by cyclin-dependent kinases (CDKs). In *Saccharomyces cerevisiae*, a single CDK, Cdc28, is necessary and sufficient for cell cycle regulation. Cdc28 (Cdk1 in mammals; Cdc2 in *S. pombe*) targets more than 200 substrates, and its activity and specificity are provided by the binding to one of nine cyclin subunits, divided in two groups, the G1 cyclins and B-type cyclins. The regulation of the different phase-specific cyclins is tightly controlled by oscillatory mechanisms that provide alternate periods of low and high levels of the different cyclin–Cdc28 activities, ensuring orderly progression through the cell cycle (Spellman et al., 1998; Orlando et al., 2008). In addition to cyclins, Cdc28 activity is regulated by the presence of Cdc28 inhibitors and by post-translational modifications (PTMs) such as phosphorylation (Mendenhall and Hodge, 1998). Transcriptional and translational regulation of Cdc28 seems to be of minor importance, given that the amount of Cdc28 is normally present at constant levels (and in excess) throughout the cell cycle (Mendenhall and Hodge, 1998). Cdc28 steady-state levels are promoted by Cdc37 (Farrell and Morgan, 2000), an Hsp90 co-chaperone that specifically targets protein kinases (Kimura et al., 1997). Cdc37 promotes Cdc28 folding and/or stabilization, and mediates Cdc28 activation by promoting formation of the Cdc28–Cln and Cdc28–Clb2 complexes (Mendenhall and Hodge, 1998), and is thus critical for proper cell cycle progression.

Cdc28 controls the timing of mitotic commitment, DNA replication and repair, spindle formation, chromosome separation and cytokinesis (Mendenhall and Hodge, 1998). It also affects processes not directly associated with the cell cycle, but coordinated with it, such as cell growth and bud morphogenesis (McCusker et al., 2007), lipid synthesis (Kurat et al., 2009), carbohydrate metabolism (Ewald et al., 2016) and vacuole inheritance (Peng and Weisman, 2008). Cdc28 has also been reported to impact on mitochondrial DNA (mtDNA) stability (Devin et al., 1990; Koltovaya et al., 1998) and to favour mitochondrial protein import and bioenergetic activity at G2/M phase (Harbauer et al., 2014).

Mitochondria play a number of key roles in eukaryotic cells, including ATP synthesis by oxidative phosphorylation (OXPHOS). The OXPHOS system is composed of four respiratory chain complexes, which are responsible for electron transport and generation of a proton gradient across the inner mitochondrial membrane, and the ATP synthase uses this proton gradient to drive the aerobic synthesis of ATP. *S. cerevisiae* is tolerant to mutations that inactivate the electron transport chain or OXPHOS due to its good fermenting capacity. In fact, this species can tolerate a partial deletion or complete loss of mtDNA when grown on a fermentable carbon source. Even so, the mitochondrial compartment is essential for yeast cell growth as it is required for essential biosynthetic pathways, such as amino acid synthesis and iron-sulfur cluster biogenesis (Lill et al., 2012). It is therefore not surprising that severe defects in mitochondrial inheritance trigger a checkpoint that inhibits cytokinesis (García-Rodríguez et al., 2009). Plus, cells that have lost their mtDNA (*rho0* cells) exhibit defects in G1 to S progression (Crider et al., 2012). Taken together, these pieces of evidence point to a two-way communication between mitochondrial function and cell cycle progression.

Here, we report that mitochondrial OXPHOS mutations inhibit growth in Cdc28 conditional mutants by impairing the activity of the Hsp90 co-chaperone Cdc37 and further compromising Cdc28 levels. This work presents mitochondrial dysfunction as a new factor affecting Cdc37 activity, expanding our knowledge on the complex networks involved in cell division decisions.

[1]i3S - Instituto de Investigação e Inovação em Saúde, Universidade do Porto, 4200-135 Porto, Portugal. [2]IBMC - Instituto de Biologia Celular e Molecular, Universidade do Porto, 4200-135 Porto, Portugal. [3]ICBAS - Instituto de Ciências Biomédicas Abel Salazar, Universidade do Porto, 4050-313 Porto, Portugal.
*These authors contributed equally to this work

‡Author for correspondence (clara.pereira@ibmc.up.pt)

A.C.L., 0000-0002-6292-3666; T.S.M., 0000-0001-8715-902X; V.T., 0000-0002-2179-2946; V.C., 0000-0002-7868-4663; C.P., 0000-0002-8167-6912

Handling Editor: David Glover
Received 24 May 2022; Accepted 25 November 2022

Journal of Cell Science (2023) 136, jcs260279. doi:10.1242/jcs.260279

RESULTS

Mitochondrial OXPHOS defects inhibit growth of Cdc28 conditional mutants

In this study, to improve our understanding of the interplay between cell cycle regulation and mitochondrial function, we investigated the genetic interaction between *CDC28* and *ATP2*, which encode a key cell cycle regulatory kinase and the catalytic subunit of the F_oF_1-ATP synthase, respectively. In the presence of glucose, yeast cells generate ATP primarily by glycolysis, and the presence of an intact OXPHOS is not essential for growth (Warburg, 1956). As such, to allow growth of *atp2*Δ cells, strains were cultivated on glucose-based media (fermenting conditions) throughout this work. Given that the *CDC28* gene is essential, we used a Cdc28 degron system (*cdc28td*), based on a C-terminal fusion with a heat-inducible ubiquitin ligase-target peptide (Dohmen et al., 1994), to deplete Cdc28 by shifting cells from 23°C to 37°C. Cdc28 levels after 3 h at the temperatures used in this study are shown in Fig. 1A. In fermenting conditions, wild-type (wt), *atp2*Δ, *cdc28td* and *atp2*Δ*cdc28td* cells cultured at the permissive temperature of 23°C grew similarly (Fig. 1B). However, at the semi-permissive temperature of 35°C, for which only a mild growth defect is apparent for *cdc28td* cells, a growth lethality was observed in the *atp2*Δ*cdc28td* double mutant. Reintroducing wt Cdc28 (from its natural promoter in a low-copy number vector) reverted the *atp2*Δ*cdc28td* mutant growth defects (Fig. S1). Growth defects in the *atp2*Δ*cdc28td* mutant were already evident for temperatures as low as 26°C, in which no growth defects are observed for *cdc28td* cells (Fig. 1B). At 26°C, although *cdc28td* cells exhibit normal growth, cells exhibited an altered morphology (Fig. 1B). This indicates that the *cdc28td* protein activity is suboptimal, and that potential conformational alterations in the mutant due to the presence of the degron tag not being compensated for by the increased protein levels (Fig. 1A). Absence of Atp2 aggravated the morphological alterations of *cdc28td* cells, leading to abnormally large, elongated cells even at 26°C (Fig. 1C). As growth of the *atp2*Δ single mutant is not affected under fermenting conditions, irrespective of the growth temperature, these results suggest a synergistic interaction between *CDC28* and *ATP2*.

An analysis of DNA content by flow cytometry showed that at the permissive temperature all strains showed normal distribution in the cell cycle. Although depletion of Cdc28 is expected to arrest the cell cycle at any given cell cycle phase (Papagiannakis et al., 2017), the *cdc28-td* strain showed a mild enrichment in cells at S phase after 4 h at the restrictive temperature (37°C). Notably,

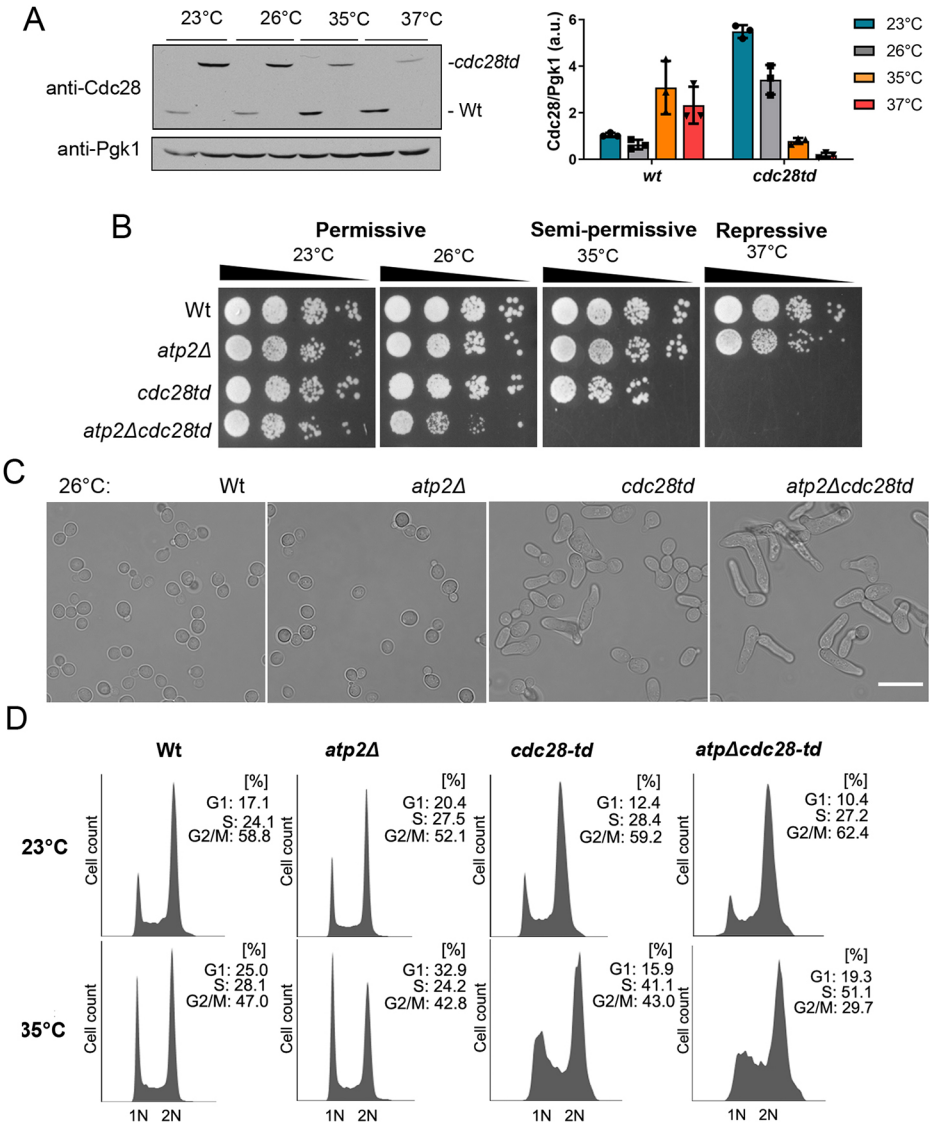

Fig. 1. *ATP2* displays a negative genetic interaction with *CDC28*. (A) Western blot showing wt Cdc28 and *cdc28td* levels in wt cells after 4 h at the indicated temperatures. Pgk1 is shown as loading control. A quantification is show on the right (mean±s.d.; *n*=4). (B) Fourfold serial dilutions of wt, *atp2*Δ, *cdc28td* (degron mutant) and *atp2*Δ*cdc28td* strains are shown after growth at the permissive, semi-permissive and restrictive temperatures, as indicated. The data shown are representative of at least three independent experiments. (C) Micrographs depicting cell morphologies of the indicated haploid strains. Cells were cultured at 26°C. Image representative of four experiments. Scale bar: 30 µm. (D) Quantitative analysis of DNA content by flow cytometry. Strains were cultured in YPD at 23°C to exponential phase and part of the same cultures was shifted at 35°C for 3 h.

Journal of Cell Science (2023) 136, jcs260279. doi:10.1242/jcs.260279

we found this S phase arrest was further aggravated by the loss of Atp2 (Fig. 1D).

Since distinct temperature-sensitive (ts) alleles of Cdc28 are available that cause arrest at specific cell cycle phases, such as G1 (*cdc28-1*) or G2/M (*cdc28-1N*) (Neiman et al., 1990; Surana et al., 1991), we tested whether lethality of *ATP2* disruption might be related to a specific cell cycle phase. We found that *ATP2* deletion also promoted a severe slow growth phenotype in *cdc28-1* and *cdc28-1N* cells (although to a lesser degree), at the respective semi-permissive conditions (Fig. 2A). Our results are consistent with Atp2 being critical for cell proliferation upon low Cdc28 activity both in G1 (Start) and mitosis. In addition, loss of Atp2 did not lead to a growth arrest at a specific cell cycle phase as it aggravated each of the *cdc28* mutant distinctive cell cycle phase arrest profiles at the permissive temperature of 26°C (Fig. 2B).

To investigate whether *ATP2* genetically interacts with additional unrelated cell cycle mutants, we introduced in *atp2*Δ cells ts mutations for the yeast Aurora kinase Ipl1 and the anaphase-promoting complex/cyclosome (APC/C) adaptor subunit Cdc20. Absence of *ATP2* did not affect the growth of either *ipl1-1* or *cdc20-1* cells at respective semi-repressive temperatures (Fig. 3A). We also found no genetic interaction between *ATP2* and the polo-like kinase-encoding gene *CDC5* (Fig. S2). These data indicate that the growth defect caused by *ATP2* deletion in *cdc28* mutants is not a phenotype shared with other cell cycle mutants. Atp2, as an essential subunit of an OXPHOS component, plays a vital role in ATP production. Yet, during growth in glucose medium, the glycolytic flux is high and the mitochondrial respiratory chain is repressed and does not contribute significantly to the cellular ATP levels (Warburg, 1956), as evidenced by the normal growth of *atp2*Δ single mutants. In addition, Atp2 might play cellular role(s) unrelated to ATP synthesis (Chen and Clark-Walker, 1999). To support the hypothesis that the negative effect of *ATP2* deletion when combined with *cdc28td* allele is related to the role of Atp2 in OXPHOS, genes encoding other ATP synthase subunits, namely *ATP1* (F1 alpha subunit) and *ATP4* (F_o subunit b) were deleted in *cdc28td* cells. Deletion of both *ATP1* and *ATP4* strongly inhibited *cdc28td* proliferation (Fig. 3B), indicating this is not a β-subunit-specific effect. We next questioned whether this phenotype was restricted to ATP synthase, or common to other OXPHOS complexes. For that, we tested the deletion of *QCR2*, a core subunit of Complex III (cytochrome bc1), and *COX4*, which encodes for a subunit of complex IV (cytochrome *c* oxidase), in *cdc28td* cells. Both *qcr2*Δ*cdc28td* and *cox4*Δ*cdc28td* strains phenocopied the *atp2*Δ*cdc28td* double mutant lethality (Fig. 3B). Ablating mitochondrial DNA in a strain carrying the *cdc28td* allele (*cdc28td rho0*) also resulted in a similar phenotype (Fig. S3). Overall, these results suggest that mitochondrial respiration in general is essential for growth of cells with reduced Cdc28 levels.

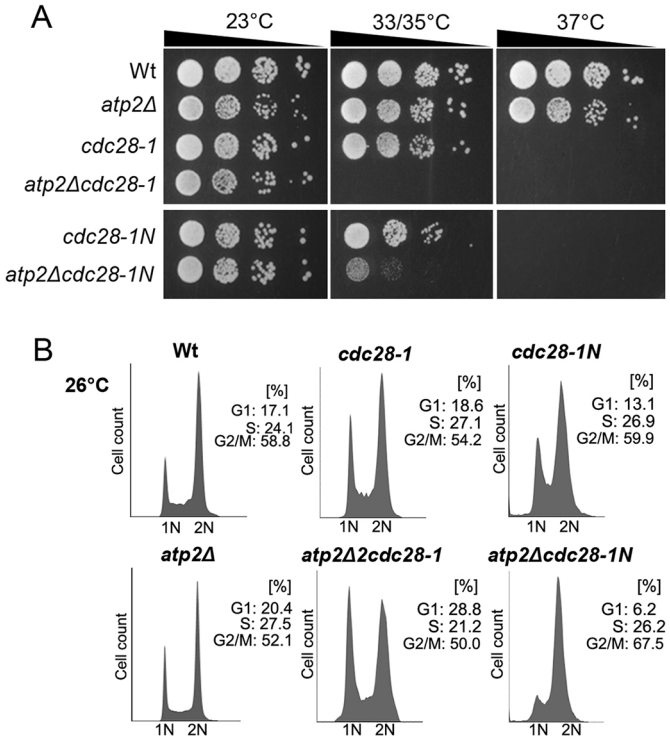

Fig. 2. *ATP2* deletion aggravate the growth defects of *cdc28-1* and *cdc28-1N ts* mutants. (A) Growth analysis of *atp2*Δ*cdc28-1* and *atp2*Δ*cdc28-1N* strains. Cells were spotted in fourfold serial dilutions and grown at permissive, semi-permissive and restrictive temperatures, as indicated. The semi-permissive temperatures used were 35°C for *cdc28-1N* mutants and 33°C for *cdc28-1*. A representative image is shown (*n*=4). (B) Cell cycle analysis by DNA content measurement. Strains were cultured at 26°C to exponential phase and analysed for DNA content by flow cytometry. Representative histograms are shown (*n*=3).

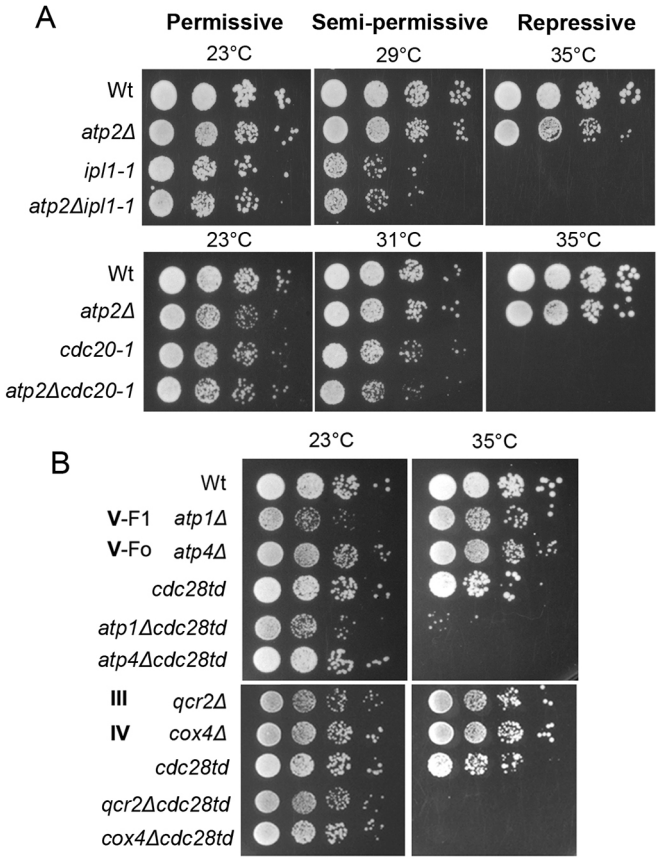

Fig. 3. *ATP2* does not interact with *IPL1* or *CDC20*, but *CDC28* shows negative genetic interactions with additional genes encoding OXPHOS components. (A) Growth analysis of *atp2*Δ*cdc20-1* and *atp2*Δ*ipl1-1* strains. Cells were spotted in fourfold serial dilutions and grown at permissive, semi-permissive and restrictive temperatures, as indicated. A representative image is shown (*n*=3). (B) Growth analysis of *atp1*Δ*cdc28td*, *atp4*Δ*cdc28td*, *qcr2*Δ*cdc28td* and *cox4*Δ*cdc28td* strains. Cells were spotted in fourfold serial dilutions and grown at permissive, semi-permissive and restrictive temperatures, as indicated. A representative image is shown (*n*=3).

Journal of Cell Science (2023) 136, jcs260279. doi:10.1242/jcs.260279

Loss of Cdc28 in the *atp2*Δ mutant aggravates mitochondrial dysfunction, but it does not trigger the retrograde response

The observed aggravating genetic interaction between OXPHOS-encoding genes and *CDC28* suggest that they have a functional relationship. Given that previous studies have indicated that Cdc28 plays a role in mitochondrial function (Devin et al., 1990; Harbauer et al., 2014), we started by addressing whether loss of Cdc28 affected mitochondrial bioenergetics (respiration and mitochondrial membrane potential) and morphology of OXPHOS mutants. For mitochondrial respiration, wt, *atp2*Δ, *cdc28td* and *atp2*Δ*cdc28td* strains cells were cultured in glucose medium to mid-log phase and incubated at the semi-permissive temperature (35°C) for 3 h. The basal oxygen consumption rate (OCR) of intact cells was then measured polarographically. The OCR was strongly reduced in *atp2*Δ and *cox4*Δ cells (2.4 and 0.8 nmol/min, respectively) compared with that found for wt cells (10 nmol/min), as anticipated. The *cdc28td* mutant, likewise *cdc28-1* or *cdc28-1N* cells (Fig. S4), exhibited an increase in OCR (16.5 nmol/min) (Fig. 4A). In addition, OCR was higher in *atp2*Δ*cdc28td* versus *atp2*Δ cells, indicating some level of mitochondrial uncoupling in the double mutant. As expected, absence of *COX4* drastically reduced the OCR in the *cdc28td* mutant since it is essential for respiration.

Next, we analysed the mitochondrial morphology of these mutants expressing a mitochondria-targeted green fluorescent protein (mtGFP), and visualized by fluorescence microscopy. In

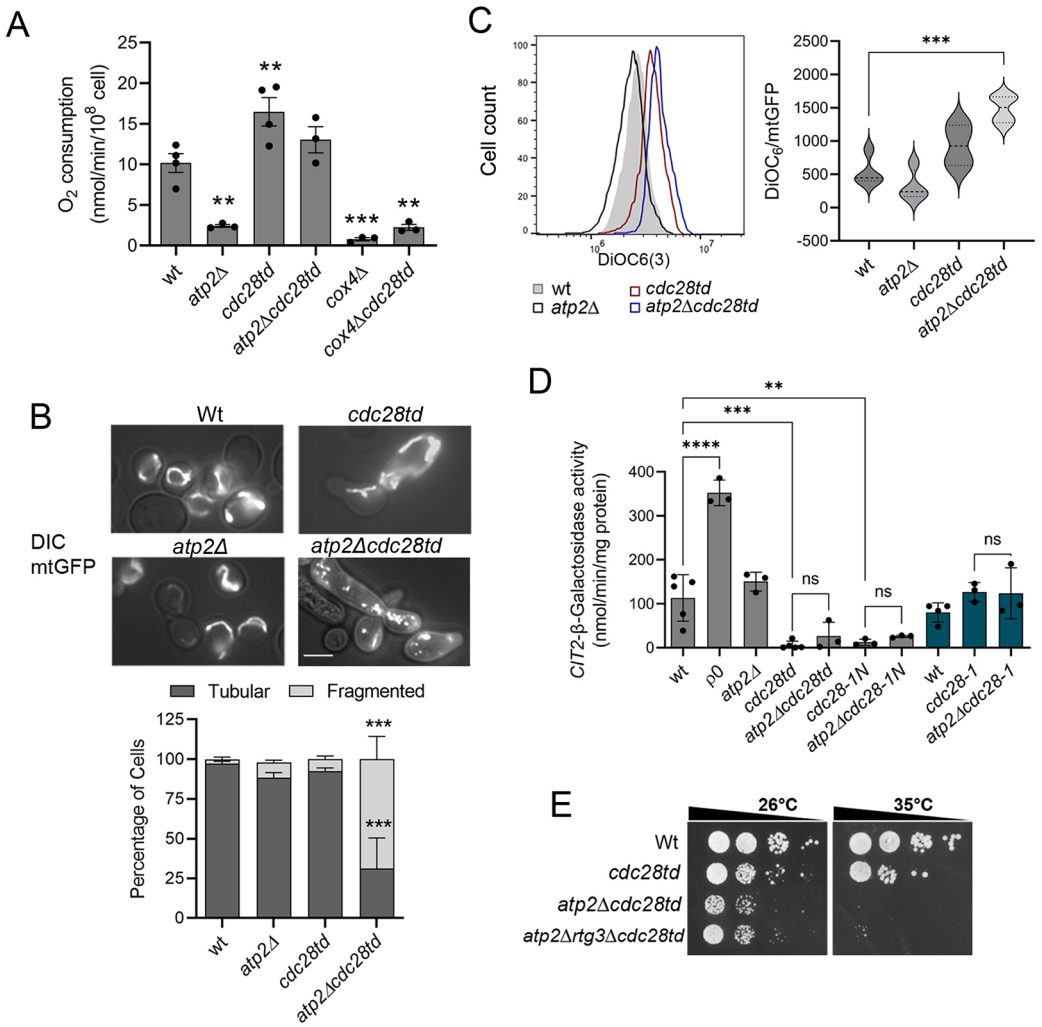

Fig. 4. Loss of Cdc28 in the *atp2*Δ mutant leads to mitochondrial defects. (A) The basal respiratory rate was determined by measuring oxygen consumption in whole cells grown in glucose medium to mid-log phase at the restrictive temperature. Values are the mean±s.d. (n=4); **P<0.01; ***P<0.001 compared with wt (one-way ANOVA followed by Tukey's multiple comparison test). (B) Yeast cells expressing mtGFP were analysed by fluorescence microscopy and mitochondrial phenotypes (tubular or fragmented) were ascertained by manually counting. Representative DIC images are merged with maximum intensity projections generated from *z*-stacks of the mitochondrial GFP signal. Scale bar: 10 µm. Values are the mean±s.d. (n=3); ***P<0.001 (one-way ANOVA followed by Tukey's multiple comparison test). (C) The indicated strains were stained with the mitochondrial membrane potential probe DiOC6(3) and analysed by flow cytometry. Images show monoparametric histograms of DiOC6(3) fluorescence [FL1 area (log)] and violin plots represent FCCP-responsive DiOC6(3) staining normalized to the mitochondrial mass. Dashed lines show the median and quartile boundaries (n=4). ***P<0.001 (one-way ANOVA followed by Šídák's multiple comparison test). (D) Activation of the retrograde pathway does not underlie the growth defects of the *atp2*Δ*cdc28td* strain. β-Galactosidase assays were carried out to determine the activity of a *CIT2-lacZ* reporter gene in *cdc28* and *atp2*Δ*cdc28* mutants, as indicated, at semi-permissive conditions (35°C for *cdc28td* and *cdc28-1N* carrying strains, in grey; 33°C for *cdc28-1* carrying strains, in blue). Cells lacking mtDNA (*rho0*) are shown as positive control. Values are the mean±s.d. (n=6); **P<0.01; ***P<0.001; ****P<0.0001; ns, not significant (one-way ANOVA followed by Tukey's multiple comparison test). (E) Growth analysis of wt, *cdc28td*, *atp2*Δ*cdc28td* and *atp2*Δ*rtg3*Δ*cdc28td*. Cells were spotted in serial dilutions and grown at indicated semi-permissive temperatures. Representative results are shown (n=3).

Journal of Cell Science (2023) 136, jcs260279. doi:10.1242/jcs.260279

agreement with previous observations, the vast majority (97%) of mitochondria in wt cells displayed a filamentous morphology. Similar results were observed in single mutants (88% for *atp2*Δ and 93% for *cdc28td* mutant). In contrast, the predominant phenotype of the *atp2*Δ*cdc28td* double mutant was punctate mitochondrial morphology (69%) indicating fragmentation (Fig. 4B; Fig. S5). We also assessed mitochondrial membrane potential (Δψm), as it reflects OXPHOS activity and is essential for mitochondrial function and biogenesis (Martin et al., 1991). The Δψm was evaluated by flow cytometry using the cationic lipophilic dye DiOC6(3), in cells incubated for 3 h in repressive conditions (35°C). Addition of the FCCP protonophore, which dissipates the Δψm, led to a substantial reduction in the DiOC6(3) uptake by all strains (Fig. S6). We used the FCCP responsive potential, eliminating unspecific binding, in the quantification of the Δψm shown in Fig. 4C. The Δψm was also normalized to the mitochondrial mass evaluated using preSU9-GFP, a mitochondrial presequence with low sensitivity to the membrane potential (Vowinckel et al., 2015). We found a significant increase (2.7-fold) of Δψm in *atp2*Δ*cdc28td* mutants, compared with that in wt cells (Fig. 4C). For the single mutant strains, no significant differences were observed. The mitochondrial localization of the fluorochrome was checked by epifluorescence microscopy and corroborated the flow cytometry results (Fig. S6). These data revealed that Cdc28 impacts on mitochondrial respiration, and loss of Cdc28 in *atp2*Δ cells leads to mitochondrial dysfunction, as indicated by the mitochondrial hyperpolarization, fragmentation and increase of uncoupled respiration.

Mitochondrial dysfunction can trigger an adaptive programme named the mitochondrial retrograde response (RTG), a pathway of communication from mitochondria to the nucleus (Butow and Avadhani, 2004). Previous studies have shown that activation of the RTG prevents cell cycle progression by upregulating Swe1, a Cdc28 inhibitor (Chen et al., 2010), and contributes to cell death during prolonged S/G2 arrest (Zyrina et al., 2015), indicating a link between RTG signalling and cell cycle. This prompted us to examine the possibility that mitochondrial dysfunction in the *atp2*Δ*cdc28td* mutant could be triggering the RTG, resulting in cell growth arrest.

The classical marker of RTG in yeast is the upregulation of *CIT2*, which encodes a glyoxylate cycle isoform of citrate synthase (Liao et al., 1991). *CIT2* induction was evaluated using a *CIT2-LacZ* reporter that was genomically integrated in the strains under study and in a *rho0* background that served as a positive control. We found that *ATP2* deletion (or *COX4* deletion, data not shown) did not induce *CIT2*-LacZ activation, either alone or in combination with the *cdc28td* allele. Similar results were observed in *cdc28-1* and *cdc28-1N* mutants lacking Atp2 (Fig. 4D). Intriguingly, LacZ activity was even lower in the *cdc28td* and *cdc28-1N* single mutants or in combination with Atp2 loss compared to that in wt, but no changes were observed in *cdc28-1* cells. Alterations in *CIT2* basal expression may be caused by the distinct cell cycle phases at which the mutants arrest, given that *CIT2* expression varies with cell cycle phases (Campbell et al., 2020; Barberis and Mondeel, 2022). Yet, as *CIT2-LacZ* activation was identical for *cdc28* single and *atp2*Δ*cdc28* double mutants, it seems unlikely that the RTG pathway is involved in the growth defects of the *atp2*Δ*cdc28* double mutant. In agreement, downregulation of the RTG pathway by deleting *RTG3* did not rescue the *atp2*Δ*cdc28td* mutant growth defects (Fig. 4E). The RTG pathway can be regulated by the levels of glutamate in the medium, whereby low glutamate levels activate and high glutamate levels repress RTG-dependent gene expression (Liu et al., 2001). Corroborating previous results, we found that growth in medium lacking or containing excess glutamate had no impact on the *atp2*Δ*cdc28td* mutant growth (Fig. S7). Overall these results show that activation of the RTG signalling pathway does not play a significant role in the lethal phenotype of the *atp2*Δ*cdc28td* mutant at semi-restrictive temperature.

OXPHOS disruption cause a strong reduction in mutant Cdc28 protein levels

Given that the cell morphology and cell cycle arrest phenotypes of *atp2*Δ*cdc28* mutants resemble an aggravated *cdc28* phenotype, we considered whether Cdc28 steady-state protein levels could be affected in the OXPHOS mutants. We evaluated wt Cdc28 and *cdc28td* levels in the absence of Atp2, Qcr2 and Cox4, in cells grown at the permissive temperature (26°C). No alterations in wt Cdc28 levels were observed in the absence of the OXPHOS proteins. However, *cdc28td* levels were noticeably lower in these cells compared with controls (Fig. 5A). This phenotype was also observed in the ts mutant *cdc28-1*, which was strongly destabilized by the absence of Atp2 (Fig. 5B). A 120-min time course analysis of *cdc28td* levels at restrictive conditions showed that Cdc28 levels decreased overtime both in *cdc28td* and *atp2*Δ*cdc28td* strains. However, in the absence of Atp2, as the Cdc28 protein level was already lower at t0, the detection limit was achieved earlier, after 1 h of incubation (Fig. 5C). Given that Cdc28 is essential for proliferation, our data suggest that the destabilization of *cdc28* upon OXPHOS disruption is the primary cause of the aggravated phenotype in the double mutant.

OXPHOS disruption in *cdc28td* cells leads to defects in the Hsp90-Cdc37 chaperone complex

Cdc28 levels are usually constant during cell division. However, Cdc28 folding and/or stabilization requires the co-chaperone Cdc37 (Farrell and Morgan, 2000), a subunit of the chaperone Hsp90 that specifically targets protein kinases (Kimura et al., 1997). Given that Cdc37 loss-of-function mutations can lead to decreased Cdc28 levels (Gerber et al., 1995), we investigated whether defects in this chaperone system could underlie the phenotype of the OXPHOS mutants carrying the *cdc28td* allele. For that, we tested the sensitivity of the strains to geldanamycin (GA), an Hsp90 inhibitor that prevents the association of Hsp90–Cdc37 complexes with client protein kinases, inhibiting their maturation (Bandhakavi et al., 2003). As shown in Fig. 6A, *atp2*Δ*cdc28td* and *cox4*Δ*cdc28td* double mutants were hypersensitive to 100 µM GA at the permissive temperature, suggesting that Hsp90–Cdc37 activity must be affected in OXPHOS/*cdc28* double mutants. Interestingly, OXPHOS and *cdc28td* single mutants exhibited a sensitivity to GA similar to wt cells.

The Hsp90–Cdc37 complex controls the folding of a large proportion of protein kinases (Mandal et al., 2007). We investigated the levels of two Hsp90–Cdc37 client kinases involved in distinct signalling pathways, Slt2 and Yck2, identified by a reduced accumulation in cells expressing a $Cdc37^{S14A}$ mutant protein (Mandal et al., 2007) that exhibits low Cdc37 activity (Bandhakavi et al., 2003). The steady-state levels of Slt2 and Yck2 were determined in wt, *atp2*Δ, *cdc28td* and *atp2*Δ*cdc28td* cells cultured at 30°C. Our results show that Slt2 and Yck2 accumulate at reduced levels in the *atp2*Δ*cdc28td* double mutant, but not in single mutants (Fig. 6B,C). This result indicates that the combination of respiratory and *cdc28* defects impacts on the stability of multiple kinase substrates of the Hsp90–Cdc37 system. We confirmed the reduced accumulation of these kinases in the $cdc37^{S14A}$ cells (Fig. 6B).

Journal of Cell Science (2023) 136, jcs260279. doi:10.1242/jcs.260279

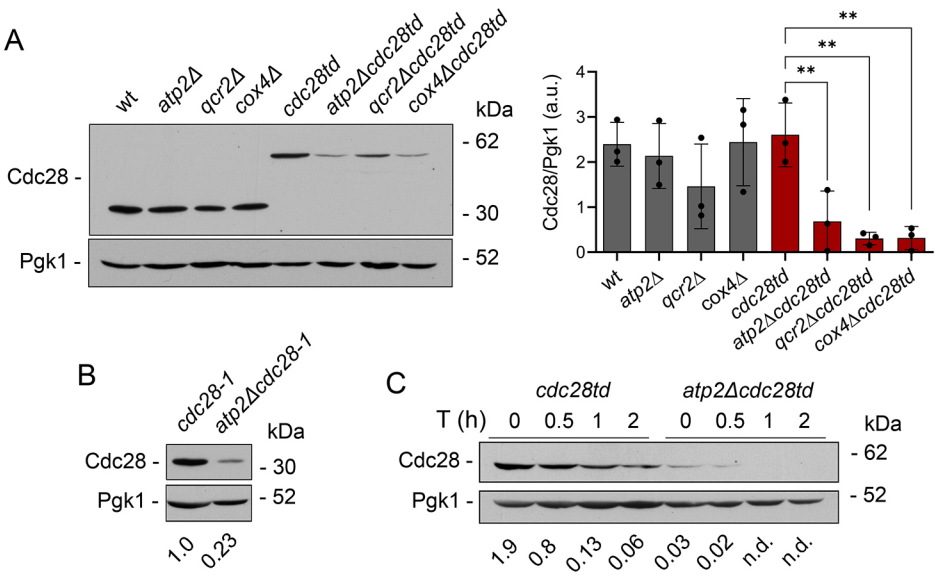

Fig. 5. Cdc28 protein levels decrease in strains combining OXPHOS defects with impaired Cdc28 activity. (A) Western blot showing wt Cdc28 and *cdc28td* levels in wt cells and in cells lacking Atp2, Qcr2 and Cox4 grown at permissive temperatures. Fold change was estimated by densitometric scanning of Cdc28 versus Pgk1 (loading control) bands. Values are the mean±s.d. (n=4); $^{**}P$<0.01 (one-way ANOVA followed by Tukey's multiple comparison test). (B) Immunodetection of Cdc28 in *cdc28-1* and *atp2Δcdc28-1* cells grown at permissive temperature. A representative blot is shown (n=3). (C) Immunodetection of Cdc28 in *cdc28td* and *atp2Δcdc28td* strains during a 120-min time course at the restrictive temperature. A representative blot is shown (n=3). Fold change is indicated.

We also investigated the levels of two kinases, Snf1 and Ypk1, whose levels were reportedly unchanged in cdc37^{S14A} cells (Mandal et al., 2007). As they are not likely Hsp90–Cdc37 targets, we predicted they would not be affected in the strains in study. Unexpectedly, Snf1 protein levels were also strongly decreased in *atp2Δcdc28td* cells in comparison with wt and single mutant strains (Fig. 6B,C). Interestingly, though not statistically significant, both Yck2 and Snf1 exhibit a tendency to accumulate at higher levels in the single *atp2Δ* mutant. Unlike Snf1, the endogenous Ypk1 levels were unchanged in *atp2Δcdc28td* cells, as expected (Fig. 6B,C).

To assess which of the Hsp90–Cdc37 complex components might be affected in the *atp2Δcdc28td* cells, we overexpressed Cdc37 and Hsp90 (encoded by *HSC82* and *HSP82* in *S. cerevisiae*) independently. Overexpression of Cdc37, the component providing kinase specificity, but not Hsc82 or Hsp82, supressed the *atp2Δcdc28td* mutant growth defects at 29°C (Fig. 7A), and had a partial protective effect at higher temperatures (32°C). Notably, the growth rescue promoted by Cdc37 overexpression in the *atp2Δcdc28td* mutant correlated with a partial restoration of Cdc28 and Snf1 levels (Fig. 7B). These results suggest that Cdc37 activity is affected in the *atp2Δcdc28td* mutant, underlying its growth defects. Notably, Cdc37 protein levels were not altered in OXPHOS mutants (single or in combination with *cdc28td*) (Fig. S8; Fig. 7B). Thus, it seems post-translational regulation of Cdc37 might be compromised in these mutant cells given that PTMs are vital for its activity (Bandhakavi et al., 2003; Shao et al., 2003). As phosphorylation on Ser14/Ser17 is essential for Cdc37 function by promoting its protein kinase-binding activity (Bandhakavi et al., 2003; Shao et al., 2003), we evaluated growth of *atp2Δcdc28td* cells

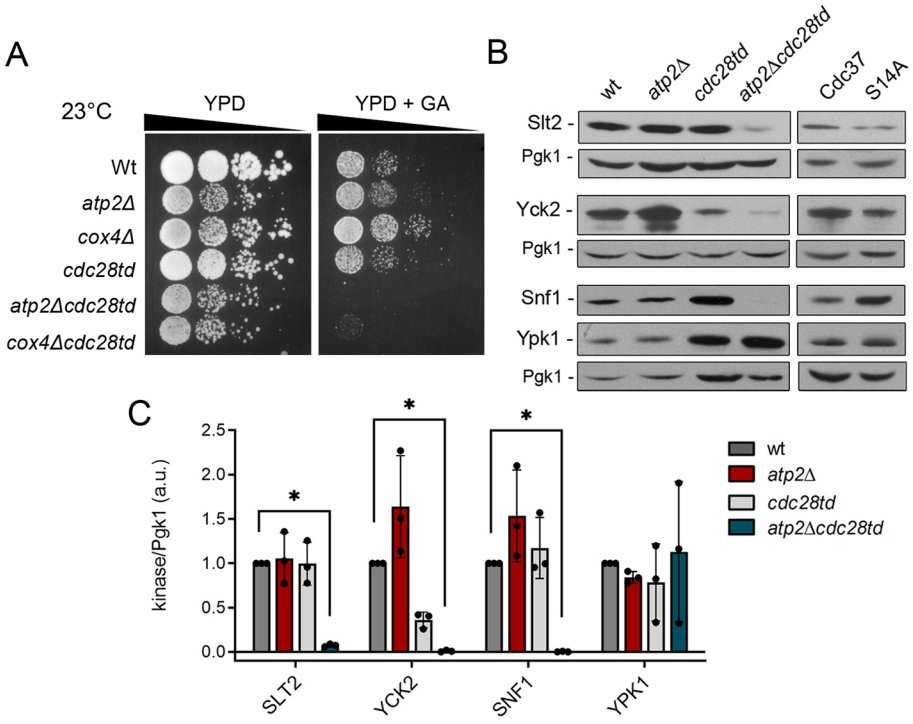

Fig. 6. Combining OXPHOS and Cdc28 mutations affect the Hsp90–Cdc37 chaperone complex. (A) Deletion of *ATP2* or *COX4* in *cdc28td* cells causes GA sensitivity in yeast. Cultures were grown at 23°C to mid-log phase, plated on YPD with solvent (DMSO) or with 100 µM GA, and incubated for 3 days at 23°C (permissive temperature). Image representative of three experiments. (B) Immunodetection of Hsp90–Cdc37 client and non-client kinases. wt, *atp2Δ*, *cdc28td atp2Δcdc28td* mutants transformed with YEp352-*SLT2–3HA*, pRS316-*SNF1-HA* and p416-*GFP-YCK2* were cultured at 30°C (semi-permissive). Slt2 and Snf1 were detected by western blot with anti-HA, Yck2 with anti-GFP and Ypk1 with anti-Ypk1. Kinase levels in wt and *cdc37*-S14A cells cultured at 30°C are shown in the right two lanes. (C) Fold change for proteins as in B was estimated by densitometric scanning of each kinase versus Pgk1 bands. Values are the mean±s.d. (n=4). $^{*}P$<0.05 (one-way ANOVA followed by Tukey's multiple comparison test).

Journal of Cell Science (2023) 136, jcs260279. doi:10.1242/jcs.260279

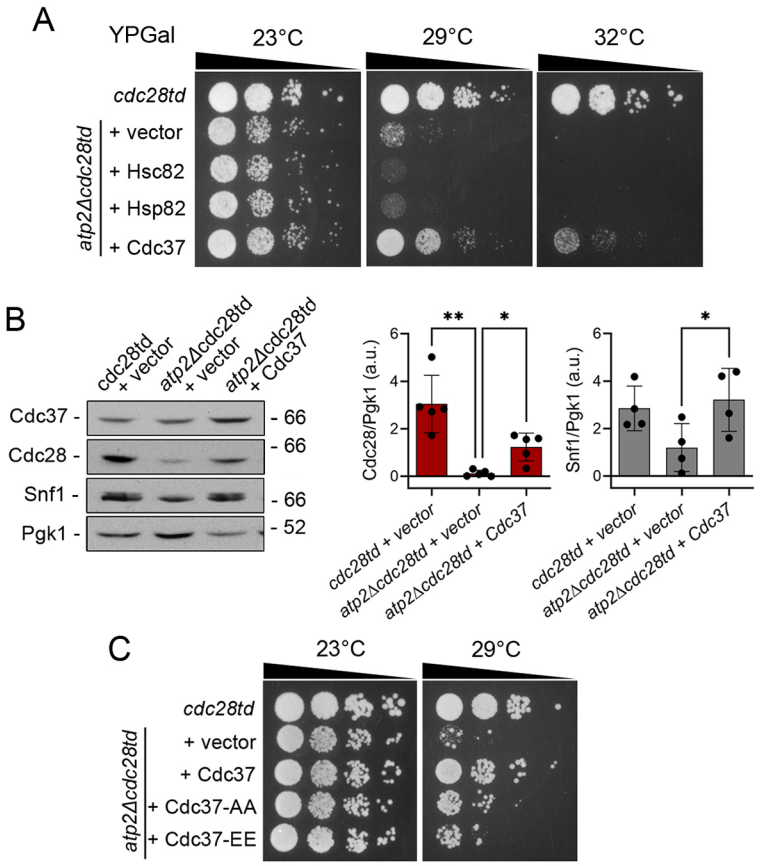

Fig. 7. Overexpression of *CDC37* partially supresses the *atp2Δcdc28td* mutant growth defects and restores Cdc28 and Snf1 levels. (A) Growth of *atp2Δcdc28td* cells overexpressing *HSC82*, *HSP82* and *CDC37* controlled by the *GAL* promoter, on galactose rich medium (YPGal) at permissive (23°C) and semi-restrictive temperatures (29°C and 32°C). (B) Western blot showing Cdc28, Snf1 and Cdc37 levels in *cdc28td* and *atp2Δcdc28td* cells transformed with empty vector or expressing Cdc37. Fold change over Pgk1 is shown on the right. Values are the mean±s.d. (n=4). *P<0.05 (one-way ANOVA followed by Tukey's multiple comparison test). (C) Growth of *atp2Δcdc28td* cells transformed with either empty vector or the plasmids expressing wt Cdc37, nonphosphorylatable Cdc37-AA (S14A/S17A) and phosphomimetic Cdc37-EE (S14E/S17E) mutants incubated at permissive and semi-restrictive temperatures. Images in A and C representative of four experiments.

transformed with either empty vector or plasmids expressing wt Cdc37, nonphosphorylatable Cdc37-S14A/S17A (Cdc37-AA) or phosphomimetic Cdc37-S14E/S17E (Cdc37-EE). Cdc37, but not Cdc37-AA or Cdc37-EE, rescued *atp2Δcdc28td* growth defects in semi-repressive conditions (Fig. 7C), suggesting that the phosphoregulation of Cdc37 is important for its protective effects.

DISCUSSION

Mitochondria are not only at the centre of aerobic energy production and essential biosynthetic activities, but are also tightly interconnected to other cellular processes and signalling cascades important for cell proliferation and survival. The present work point to a role of mitochondria in cell cycle progression by revealing that combined disturbance of mitochondrial respiration and Cdc28 activity inhibits cell proliferation. Importantly, this effect is due to inhibition of Cdc37, which in turn leads to a further decrease in Cdc28, underscoring more complex interactions between these proteins than previously anticipated. Cdc28 plays a major role in cell division and its activity is carefully controlled by checkpoint mechanisms that monitor cues from the environment and their own internal state (Mendenhall and Hodge, 1998). Our results suggest that under less than optimal conditions, when Cdc28 activity is reduced, mitochondrial fitness will be decisive for cell cycle progression decisions.

The aggravated phenotype in the OXPHOS/*cdc28* double mutants (mitochondrial fragmentation and hyperpolarization) suggests that Cdc28 might affect a pathway in common with mitochondrial respiration. Previous reports have already given evidence that Cdc28/Cdk1 is required for normal mitochondrial function in both yeast and mammals (Genta et al., 1995; Harbauer et al., 2014; Taguchi et al., 2007). In mammalian cells, Cdk1 favours mitochondrial fragmentation during mitosis by phosphorylating the dynamin-related GTPase Drp1 (yeast Dnm1) (Taguchi et al., 2007). Whether Cdc28 also targets the mitochondrial fusion/fission machinery in yeast is still unknown. Curiously, given that a repressible mutant of Cdc37 also leads to abnormal fragmentation (Altmann and Westermann, 2005), we cannot discard the hypothesis that the observed mitochondrial morphology defects in the OXPHOS/*cdc28* double mutants is a consequence, and not a cause, of Cdc37 inhibition. Apparently, mitochondrial function might affect more and be more affected by the cell cycle machinery than previously anticipated.

A remaining question is how the combined impairment of mitochondrial respiration and Cdc28 activity leads to an inhibition of Cdc37. In this work, we have discarded the hypothesis that the aggravated mitochondrial dysfunction in the OXPHOS/*cdc28* mutants triggers the RTG response. Given that we observed that Cdc37 protein levels are not altered in this strain, Cdc37 inhibition might be associated with changes at the PTM level. Cdc37 PTMs can occur in several amino acid residues, many of unknown physiological relevance, as listed in the SGD database (Hellerstedt et al., 2017). A prominent PTM is phosphorylation on S14 and/or S17 (residue S13 in the human protein), as this modification is considered essential for Cdc37 function (Bandhakavi et al., 2003; Shao et al., 2003). However, the expression of a phosphomimetic Cdc37-EE version, comparing to the phosphoresistant Cdc37-AA, did not have a protective effect on the *atp2Δcdc28td* mutant, arguing against this hypothesis. Plus, Snf1 stability decreased in the *atp2Δcdc28td* mutant (our results) but not in cdc37^{S14A} cells (Mandal et al., 2007). In our conditions, Snf1 even accumulated at higher levels in cells expressing the Cdc37-S14A mutant. Phosphorylation of S14 is normally crucial for the stabilization of Cdc37 client kinases, with exceptions. For example, Cak1 accumulates at higher levels upon loss of Cdc37-S14

Journal of Cell Science (2023) 136, jcs260279. doi:10.1242/jcs.260279

phosphorylation (Millson et al., 2014). It is conceivable that PTMs other than S14 phosphorylation might impact on the Cdc37 activity towards specific kinases.

Expanding our knowledge on the complex interactions between mitochondrial dysfunction and impaired kinase activity will improve our understanding of the multifactorial interactions controlling proliferation and potentially disease. In humans, a prominent number of Cdc37 targets are oncoproteins (Miyata and Nishida, 2004) and aberrant CDK activity also underpins proliferation of tumour cells (Malumbres and Barbacid, 2009), making research on the regulation of these proteins of considerable interest. Plus, mitochondrial metabolism is altered in cancer cells and OXPHOS inhibitors are gaining attention as therapeutic approaches (Ashton et al., 2018). Given that inhibition of both Cdc28 and OXPHOS have a strong growth inhibitory effect in our model, we postulate that the synergistic use of CDK and OXPHOS inhibitors might also be advantageous in antitumour therapeutics.

MATERIALS AND METHODS

Yeast strains and growth conditions

The *S. cerevisiae* strains used in this study are all BY4741 derivative and are listed in Table S1. The *atp1*Δ, *atp4*Δ, *qcr2*Δ and *cox4*Δ strains were constructed by replacing the open-reading frame (ORF) of each gene with the auxotroph marker *HIS3*, using PCR-mediated homologous recombination. To construct double mutant strains, the cassette containing *cdc28td:KanMX4*, *cdc28-1:KanMX4*, *cdc20-1:KanMX4* and *ipl1-1:KanMX4* were amplified by PCR and transformed in indicated deletion strains. To construct the *cdc28-1N*-expressing strains, the *cdc28-1N* sequence was amplified from the US102 strain (Loy et al., 1999) and fused to the KanMX6 cassette, using overlap extension PCR. This product was then integrated into wt and *atp2*Δ strains. pBL101-p*CIT2*-LacZ (Liu and Butow, 1999) was linearized by digestion with *Sma*I and integrated into the genomic *CIT2* locus. Correct deletions/insertions were confirmed by PCR. For Hsp90 and Cdc37 overexpression, the auxotroph marker *HIS3* in the *atp2*Δ*cdc28td* strain was replaced by *URA3* by PCR-mediated recombination, and cells were transformed with empty vector, pAG423*GAL-HSC82*, pAG423*GAL-HSP82* or pAG423*GAL-CDC37* (Lin et al., 2021). For kinase levels assays, wt, *atp2*Δ, *cdc28td*, *atp2*Δ*cdc28td* cells were transformed with YEp352-*SLT2-3HA* (Madden et al., 1997), pRS316-*SNF1-HA* (Ye et al., 2008) and p416-ADH-yeGFP-*YCK2*. To generate p416-ADH-yeGFP-*YCK2*, the yeGFP sequence was inserted into the *Xba*I site of the p416ADH plasmid followed by insertion of the *YCK2* sequence (*Bam*HI-*Sal*I fragment) amplified. Strains TM141 *cdc37*Δ::*HIS3* [Ycplac111 CDC37-HA] and *cdc37*Δ::*HIS3* [Ycplac111 *CDC37-S14A-HA*] (Hawle et al., 2007) were also transformed with the above plasmids and used as control. For growth assays, Ycplac111-*CDC37*, *CDC37S14/17A* and *CDC37S14/17E* were isolated from TM141 strains (Vaughan et al., 2008) and plasmids used to transform *cdc28td* and *atp2*Δ*cdc28td* cells.

Strains were transformed by the standard lithium acetate procedure (Gietz and Schiestl, 2007). To avoid clonal variability, at least two different colonies were analysed in all experiments.

Cells were grown in YPD rich medium [1% (w/v) yeast extract, 2% (w/v) peptone and 2% (w/v) glucose; Thermo Fisher Scientific]. YPGal/Raf containing 2% (w/v) galactose (Biosynth) plus 2% (w/v) raffinose (Biosynth) instead of glucose as a carbon source, was used for the induction of gene expression from plasmids with the *GAL1* promoter. Cultures were routinely grown in an orbital shaker at 140 rpm.

For clone selection, strains were grown in YPD agar supplemented with 250 µg/ml geneticin (Santa Cruz Biotechnology) or in synthetic complete medium [SC; 0.67% (w/v) Bacto-yeast nitrogen base without amino acids (BD Difco), 2% (w/v) glucose and 0.2% (w/v) dropout mix; Sigma] lacking histidine or uracil, as appropriate.

For geldanamycin (GA; MedChemExpress)-supplemented medium, GA was dissolved in dimethyl sulfoxide and added to a final concentration of 100 µM to warm YPD agar medium before pouring.

All strains are available upon request.

β-galactosidase assay

For the β-galactosidase assay, yeast cells expressing *pCIT2-LacZ* were grown in YPD to exponential phase. Cells were incubated for 3 h at the restrictive temperature to inactivate *cdc28td* (37°C), *cdc28-1N* (37°C) and *cdc28-1* (35°C). The β-galactosidase activity was measured in a liquid assay using o-nitrophenyl-β-D-galactoside (ONPG) as previously described (Almeida et al., 2008), using 60 µg of total protein.

Cell cycle analysis

For cell cycle analysis, strains were cultured overnight in YPD at 24°C to mid-log phase. A portion of the cultures was then shifted to 37°C for 3 h, while the remaining was maintained at 24°C for the same time and used as the control. Cells were fixed overnight and DNA content was analysed by flow cytometry using 10 µM SYTOX Green (Molecular Probes), basically as described in Haase and Reed (2002). Cells were analysed using the FL1 detector in a BD Accuri C6. 20,000 events were analysed per sample and cell cycle distribution was estimated using FlowJo v10 software version.

Mitochondrial membrane potential

To assess the mitochondrial membrane potential ($\Delta\Psi m$), cells were incubated for 30 min at 30°C with 40 nM of 3,3 dihexyloacarbocynine iodide [DiOC6(3); Molecular Probes; Pereira et al., 2014]. When used, the uncoupler carbonyl-cyanide 4-(trifluoromethoxy)-phenylhydrazone (FCCP, Sigma; 10 µM) was added 10 min before loading with DiOC6(3). At least 20,000 cells were analysed per sample using the FL1 detector in a BD Accuri C6 flow cytometer. The collected data was analysed using FlowJo v10 software version to determine the mean green fluorescence intensity.

Oxygen consumption rate

The oxygen consumption rate was measured polarographically in whole cells (10^8 in PBS buffer) from cultures grown in YPD medium to late log phase, using a Clark-type oxygen electrode coupled to an Oxygraph plus system (Hansatech). Data were analysed using the OxyTrace$^+$ software. The respiratory rate in the presence and absence of the inhibitor potassium cyanide (700 µM; Merck) was obtained by dividing the oxygen consumed per min by the number of cells used in the experiment.

Microscopy analysis

For the analysis of mitochondrial morphology and volume, samples from strains transformed with a pVT100mtGFP fusion gene (Westermann and Neupert, 2000) were imaged by fluorescence microscopy. Images were acquired by epifluorescence in a Zeiss Axio Imager Z1 microscope fitted with Nomarski optics with an Axiocam MR3.0 camera and analysed using the Axiovision 4.7 software. Images were collected at 0.4 µm *z*-intervals and average projected to produce the final image. The mitochondria morphology types were analysed manually in ∼100 cells per strain, and the mitochondrial area in the cell was measured using the tools included in the ImageJ software (NIH).

Immunoblotting

Yeast total protein lysates were obtained by boiling in SDS sample buffer (without β-mercapthoethanol) at 95°C (5 min). Protein concentration was measured using the Pierce BCA Protein Assay Kit (Thermo Fisher Scientific) and β-mercapthoethanol was then added to the lysate. Proteins (40 µg) were separated by SDS-PAGE, electroblotted onto a nitrocellulose membrane (Hybond-C, GE Healthcare) and probed with antibodies using standard protocols. Primary antibodies used were anti-Cdc28 (1:150; sc-515762, Santa Cruz Biotechnology), anti-Cdc37 (1:15,000; ab188280, Abcam), anti-Ypk1 (1:500; sc-12051, Santa Cruz Biotechnology), anti-Snf1 (1:100; sc-15622, Santa Cruz Biotechnology), anti-Pgk1 (1:25,000; 22C5D8, Thermo Fisher Scientific), anti-GFP (1:6000; Clontech), and anti-HA (1:5000; sc-7392, Santa Cruz Biotechnology). Secondary antibodies used were anti-mouse IgG-HRP (1:7000, Molecular probes), anti-rabbit IgG-HRP (1:7000, Sigma) and anti-goat IgG-HRP (1:5000, Santa Cruz Biotechnology). Membranes were washed, incubated with WesternBright ECL (Advansta), exposed to LucentBlue X-ray film (Advansta), and scanned on a Molecular Imager GS800. Protein band intensities were

quantified using Quantity One 1-D Analysis Software version 4.6 (Bio-Rad).

Full-length blots corresponding to the blots displayed in various figures and showing molecular mass markers are provided in Fig. S9.

Acknowledgements
We are very grateful to Uttam Surana (A*STAR, Singapore) for the *cdc28-1N* strain, Zhengchang Liu (University of New Orleans, LA, USA) for the *CIT2-LacZ* plasmid, John Pringle (Stanford University School of Medicine, CA, USA) for the pFA6a-kanMX6-PGAL1-3HA plasmid, and Martin L. Duennwald (University of Western Ontario, Canada) for the *CDC37*, *HSC82* and *HSP82* overexpression plasmids. The Cdc37 (WT), cdc37S14A, cdc37S14/17A, and cdc37S14/17E strains were generously provided by Marco Siderius (Vrije Universiteit Amsterdam, Netherlands) and Mehdi Mollapour (Upstate Medical University, NY, USA). The authors acknowledge the support of the i3S Scientific Platforms Translational Cytometry and Advanced Light Microscopy (member of the national infrastructure PPBI - Portuguese Platform of Bioimaging PPBI-POCI-01-0145-FEDER-022122).

Competing interests
The authors declare no competing or financial interests.

Author contributions
Conceptualization: V.C., C.P.; Formal analysis: V.C., C.P.; Investigation: A.C.L., T.S.M., R.R.C., V.T., C.P.; Resources: V.C.; Writing - original draft: C.P.; Writing - review & editing: A.C.L., T.S.M., R.R.C., V.T., V.C., C.P.; Supervision: C.P.; Project administration: C.P.; Funding acquisition: V.C., C.P.

Funding
This work was funded by national funds through Fundação para a Ciência e a Tecnologia (FCT), I.P., under the project UIDB/04293/2020. T.S.M. (SFRH/BD/136996/2018) and A.C.L. (SFRH/BD/135921/2018) are recipients of FCT fellowships. C.P. is supported by Fundo Social Europeu and Programa Operacional Potencial Humano through FCT investigator grant IF/00889/2015.

Data availability
All relevant data can be found within the article and its supplementary information.

Peer review history
The peer review history is available online at https://journals.biologists.com/jcs/lookup/doi/10.1242/jcs.260279.reviewer-comments.pdf

References
Almeida, T., Marques, M., Mojzita, D., Amorim, M. A., Silva, R. D., Almeida, B., Rodrigues, P., Ludovico, P., Hohmann, S., Moradas-Ferreira, P. et al. (2008). Isc1p plays a key role in hydrogen peroxide resistance and chronological lifespan through modulation of iron levels and apoptosis. *Mol. Biol. Cell* **19**, 865-876. doi:10.1091/mbc.e07-06-0604

Altmann, K. and Westermann, B. (2005). Role of essential genes in mitochondrial morphogenesis in *Saccharomyces cerevisiae*. *Mol. Biol. Cell* **16**, 5410-5417. doi:10.1091/mbc.e05-07-0678

Ashton, T. M., McKenna, W. G., Kunz-Schughart, L. A. and Higgins, G. S. (2018). Oxidative phosphorylation as an emerging target in cancer therapy. *Clin. Cancer Res.* **24**, 2482-2490. doi:10.1158/1078-0432.CCR-17-3070

Bandhakavi, S., McCann, R. O., Hanna, D. E. and Glover, C. V. C. (2003). A positive feedback loop between protein kinase CKII and Cdc37 promotes the activity of multiple protein kinases. *J. Biol. Chem.* **278**, 2829-2836. doi:10.1074/jbc.M206662200

Barberis, M. and Mondeel, T. D. G. A. (2022). Unveiling Forkhead-mediated regulation of yeast cell cycle and metabolic networks. *Comput. Struct. Biotechnol. J.* **20**, 1743-1751. doi:10.1016/j.csbj.2022.03.033

Butow, R. A. and Avadhani, N. G. (2004). Mitochondrial signaling: the retrograde response. *Mol. Cell* **14**, 1-15. doi:10.1016/S1097-2765(04)00179-0

Campbell, K., Westholm, J., Kasvandik, S., Di Bartolomeo, F., Mormino, M. and Nielsen, J. (2020). Building blocks are synthesized on demand during the yeast cell cycle. *Proc. Natl. Acad. Sci. USA* **117**, 7575-7583. doi:10.1073/pnas.1919535117

Chen, X. J. and Clark-Walker, G. D. (1999). α and β subunits of F1-ATPase are required for survival of petite mutants in *Saccharomyces cerevisiae*. *Mol. Gen. Genet.* **262**, 898-908. doi:10.1007/s004380051156

Chen, S., Liu, D., Finley, R. L., Jr. and Greenberg, M. L. (2010). Loss of mitochondrial DNA in the yeast cardiolipin synthase crd1 mutant leads to up-regulation of the protein kinase Swe1p that regulates the G2/M transition. *J. Biol. Chem.* **285**, 10397-10407. doi:10.1074/jbc.M110.100784

Crider, D. G., García-Rodríguez, L. J., Srivastava, P., Peraza-Reyes, L., Upadhyaya, K., Boldogh, I. R. and Pon, L. A. (2012). Rad53 is essential for a mitochondrial DNA inheritance checkpoint regulating G1 to S progression. *J. Cell Biol.* **198**, 793-798. doi:10.1083/jcb.201205193

Devin, A. B., Prosvirova, T. Y., Peshekhonov, V. T., Chepurnaya, O. V., Smirnova, M. E., Koltovaya, N. A., Troitskaya, E. N. and Arman, I. P. (1990). The start gene CDC28 and the genetic stability of yeast. *Yeast* **6**, 231-243. doi:10.1002/yea.320060308

Dohmen, R. J., Wu, P. and Varshavsky, A. (1994). Heat-inducible degron: a method for constructing temperature-sensitive mutants. *Science* **263**, 1273-1276. doi:10.1126/science.8122109

Ewald, J. C., Kuehne, A., Zamboni, N. and Skotheim, J. M. (2016). The yeast cyclin-dependent kinase routes carbon fluxes to fuel cell cycle progression. *Mol. Cell* **62**, 532-545. doi:10.1016/j.molcel.2016.02.017

Farrell, A. and Morgan, D. O. (2000). Cdc37 promotes the stability of protein kinases Cdc28 and Cak1. *Mol. Cell Biol.* **20**, 749-754. doi:10.1128/MCB.20.3.749-754.2000

García-Rodríguez, L. J., Crider, D. G., Gay, A. C., Salanueva, I. J., Boldogh, I. R. and Pon, L. A. (2009). Mitochondrial inheritance is required for MEN-regulated cytokinesis in budding yeast. *Curr. Biol.* **19**, 1730-1735. doi:10.1016/j.cub.2009.08.041

Genta, H. D., Mónaco, M. E. and Aon, M. A. (1995). Decreased mitochondrial biogenesis in temperature-sensitive cell division cycle mutants of *Saccharomyces cerevisiae*. *Curr. Microbiol.* **31**, 327-331. doi:10.1007/BF00294693

Gerber, M. R., Farrell, A., Deshaies, R. J., Herskowitz, I. and Morgan, D. O. (1995). Cdc37 is required for association of the protein kinase Cdc28 with G1 and mitotic cyclins. *Proc. Natl. Acad. Sci. USA* **92**, 4651-4655. doi:10.1073/pnas.92.10.4651

Gietz, R. D. and Schiestl, R. H. (2007). High-efficiency yeast transformation using the LiAc/SS carrier DNA/PEG method. *Nat. Protoc.* **2**, 31-34. doi:10.1038/nprot.2007.13

Haase, S. B. and Reed, S. I. (2002). Improved flow cytometric analysis of the budding yeast cell cycle. *Cell Cycle* **1**, 132-136. doi:10.4161/cc.1.2.114

Harbauer, A. B., Opalińska, M., Gerbeth, C., Herman, J. S., Rao, S., Schönfisch, B., Guiard, B., Schmidt, O., Pfanner, N. and Meisinger, C. (2014). Cell cycle–dependent regulation of mitochondrial preprotein translocase. *Science* **346**, 1109-1113. doi:10.1126/science.1261253

Hawle, P., Horst, D., Bebelman, J. P., Yang, X. X., Siderius, M. and van der Vies, S. M. (2007). Cdc37p is required for stress-induced high-osmolarity glycerol and protein kinase C mitogen-activated protein kinase pathway functionality by interaction with Hog1p and Slt2p (Mpk1p). *Eukaryot. Cell* **6**, 521-532. doi:10.1128/EC.00343-06

Hellerstedt, S. T., Nash, R. S., Weng, S., Paskov, K. M., Wong, E. D., Karra, K., Engel, S. R. and Cherry, J. M. (2017). Curated protein information in the Saccharomyces genome database. *Database,* **2017**, bax011. doi:10.1093/database/bax011

Kimura, Y., Rutherford, S. L., Miyata, Y., Yahara, I., Freeman, B. C., Yue, L., Morimoto, R. I. and Lindquist, S. (1997). Cdc37 is a molecular chaperone with specific functions in signal transduction. *Genes Dev.* **11**, 1775-1785. doi:10.1101/gad.11.14.1775

Koltovaya, N. A., Arman, I. P. and Devin, A. B. (1998). Mutations of the CDC28 gene and the radiation sensitivity of *Saccharomyces cerevisiae*. *Yeast* **14**, 133-146. doi:10.1002/(SICI)1097-0061(19980130)14:2<133::AID-YEA206>3.0.CO;2-0

Kurat, C. F., Wolinski, H., Petschnigg, J., Kaluarachchi, S., Andrews, B., Natter, K. and Kohlwein, S. D. (2009). Cdk1/Cdc28-dependent activation of the major triacylglycerol lipase Tgl4 in yeast links lipolysis to cell-cycle progression. *Mol. Cell* **33**, 53-63. doi:10.1016/j.molcel.2008.12.019

Liao, X. S., Small, W. C., Srere, P. A. and Butow, R. A. (1991). Intramitochondrial functions regulate nonmitochondrial citrate synthase (Cit2) expression in *Saccharomyces cerevisiae*. *Mol. Cell Biol.* **11**, 38-46. doi:10.1128/mcb.11.1.38-46.1991

Lill, R., Hoffmann, B., Molik, S., Pierik, A. J., Rietzschel, N., Stehling, O., Uzarska, M. A., Webert, H., Wilbrecht, C. and Muhlenhoff, U. (2012). The role of mitochondria in cellular iron-sulfur protein biogenesis and iron metabolism. *Biochim. Biophys. Acta Mol. Cell Res.* **1823**, 1491-1508. doi:10.1016/j.bbamcr.2012.05.009

Lin, L. T.-W., Razzaq, A., Di Gregorio, S. E., Hong, S., Charles, B., Lopes, M. H., Beraldo, F., Prado, V. F., Prado, M. A. M. and Duennwald, M. L. (2021). Hsp90 and its co-chaperone Sti1 control TDP-43 misfolding and toxicity. *FASEB J.* **35**, e21594. doi:10.1096/fj.202002645R

Liu, Z. C. and Butow, R. A. (1999). A transcriptional switch in the expression of yeast tricarboxylic acid cycle genes in response to a reduction or loss of respiratory function. *Mol. Cell Biol.* **19**, 6720-6728. doi:10.1128/MCB.19.10.6720

Liu, Z., Sekito, T., Epstein, C. B. and Butow, R. A. (2001). RTG-dependent mitochondria to nucleus signaling is negatively regulated by the seven WD-repeat protein Lst8p. *EMBO J.* **20**, 7209-7219. doi:10.1093/emboj/20.24.7209

Loy, C. J., Lydall, D. and Surana, U. (1999). NDD1, a high-dosage suppressor of cdc28-1N, is essential for expression of a subset of late-S-phase-specific genes in *Saccharomyces cerevisiae*. *Mol. Cell Biol.* **19**, 3312-3327. doi:10.1128/MCB.19.5.3312

Madden, K., Sheu, Y.-J., Baetz, K., Andrews, B. and Snyder, M. (1997). SBF cell cycle regulator as a target of the yeast PKC-MAP kinase pathway. *Science* **275**, 1781-1784. doi:10.1126/science.275.5307.1781

Malumbres, M. and Barbacid, M. (2009). Cell cycle, CDKs and cancer: a changing paradigm. *Nat. Rev. Cancer* **9**, 153-166. doi:10.1038/nrc2602

Mandal, A. K., Lee, P., Chen, J. A., Nillegoda, N., Heller, A., DiStasio, S., Oen, H., Victor, J., Nair, D. M., Brodsky, J. L. et al. (2007). Cdc37 has distinct roles in protein kinase quality control that protect nascent chains from degradation and promote posttranslational maturation. *J. Cell Biol.* **176**, 319-328. doi:10.1083/jcb.200604106

Martin, J., Mahlke, K. and Pfanner N. (1991). Role of an energized inner membrane in mitochondrial protein import. Delta psi drives the movement of presequences. *J. Biol. Chem.* **266**, 18051-18057. doi:10.1074/jbc.M607551200

McCusker, D., Denison, C., Anderson, S., Egelhofer, T. A., Yates, J. R., III, Gygi, S. P. and Kellogg, D. R. (2007). Cdk1 coordinates cell-surface growth with the cell cycle. *Nat. Cell Biol.* **9**, 506-515. doi:10.1038/ncb1568

Mendenhall, M. D. and Hodge, A. E. (1998). Regulation of Cdc28 cyclin-dependent protein kinase activity during the cell cycle of the yeast *Saccharomyces cerevisiae*. *Microbiol. Mol. Biol. Rev.* **62**, 1191-1243. doi:10.1128/MMBR.62.4.1191-1243.1998

Millson, S., van Oosten-Hawle, P., Alkuriji, M. A., Truman, A., Siderius, M. and Piper, P. W. (2014). Cdc37 engages in stable, S14A mutation-reinforced association with the most atypical member of the yeast kinome, Cdk-activating kinase (Cak1). *Cell Stress Chaperon.* **19**, 695-703. doi:10.1007/s12192-014-0497-4

Miyata, Y. and Nishida, E. (2004). Supervision of multiple signaling protein kinases by the CK2-Cdc37 couple, a possible novel cancer therapeutic target. *Ann. N. Y. Acad. Sci.* **1030**, 150-157. doi:10.1196/annals.1329.019

Neiman, A. M., Chang, F., Komachi, K. and Herskowitz, I. (1990). Cdc36 and Cdc39 are negative elements in the signal transduction pathway of yeast. *Cell Regul.* **1**, 391-401. doi:10.1091/mbc.1.5.391

Orlando, D. A., Lin, C. Y., Bernard, A., Wang, J. Y., Socolar, J. E. S., Iversen, E. S., Hartemink, A. J. and Haase, S. B. (2008). Global control of cell-cycle transcription by coupled CDK and network oscillators. *Nature* **453**, 944-947. doi:10.1038/nature06955

Papagiannakis, A., de Jonge, J. J., Zhang, Z. and Heinemann, M. (2017). Quantitative characterization of the auxin-inducible degron: a guide for dynamic protein depletion in single yeast cells. *Sci. Rep.* **7**, 4704. doi:10.1038/s41598-017-04791-6

Peng, Y. and Weisman, L. S. (2008). The cyclin-dependent kinase Cdk1 directly regulates vacuole inheritance. *Dev. Cell* **15**, 478-485. doi:10.1016/j.devcel.2008.07.007

Pereira, C., Miguel Martins, L. and Saraiva, L. (2014). LRRK2, but not pathogenic mutants, protects against H2O2 stress depending on mitochondrial function and endocytosis in a yeast model. *Biochim. Biophys. Acta Gen. Subj.* **1840**, 2025-2031. doi:10.1016/j.bbagen.2014.02.015

Shao, J. Y., Prince, T., Hartson, S. D. and Matts, R. L. (2003). Phosphorylation of serine 13 is required for the proper function of the Hsp90 co-chaperone, Cdc37. *J. Biol. Chem.* **278**, 38117-38120. doi:10.1074/jbc.C300330200

Spellman, P. T., Sherlock, G., Zhang, M. Q., Iyer, V. R., Anders, K., Eisen, M. B., Brown, P. O., Botstein, D. and Futcher, B. (1998). Comprehensive identification of cell cycle–regulated genes of the yeast *Saccharomyces cerevisiae* by microarray hybridization. *Mol. Cell Biol.* **9**, 3273-3297. doi:10.1091/mbc.9.12.3273

Surana, U., Robitsch, H., Price, C., Schuster, T., Fitch, I., Futcher, A. B. and Nasmyth, K. (1991). The role of CDC28 and cyclins during mitosis in the budding yeast *S. cerevisiae*. *Cell* **65**, 145-161. doi:10.1016/0092-8674(91)90416-V

Taguchi, N., Ishihara, N., Jofuku, A., Oka, T. and Mihara, K. (2007). Mitotic phosphorylation of Dynamin-related GTPase Drp1 participates in mitochondrial fission. *J. Biol. Chem.* **282**, 11521-11529. doi:10.1074/jbc.M607279200

Vaughan, C. K., Mollapour, M., Smith, J. R., Truman, A., Hu, B., Good, V. M., Panaretou, B., Neckers, L., Clarke, P. A., Workman, P. et al. (2008). Hsp90-dependent activation of protein kinases is regulated by chaperone-targeted dephosphorylation of Cdc37. *Mol. Cell* **31**, 886-895. doi:10.1016/j.molcel.2008.07.021

Vowinckel, J., Hartl, J., Butler, R. and Ralser, M. (2015). MitoLoc: A method for the simultaneous quantification of mitochondrial network morphology and membrane potential in single cells. *Mitochondrion* **24**, 77-86. doi:10.1016/j.mito.2015.07.001

Warburg, O. (1956). On the origin of cancer cells. *Science* **123**, 309-314. doi:10.1126/science.123.3191.309

Westermann, B. and Neupert, W. (2000). Mitochondria-targeted green fluorescent proteins: convenient tools for the study of organelle biogenesis in *Saccharomyces cerevisiae*. *Yeast* **16**, 1421-1427. doi:10.1002/1097-0061(200011)16:15<1421::AID-YEA624>3.0.CO;2-U

Ye, T., Elbing, K. and Hohmann, S. (2008). The pathway by which the yeast protein kinase Snf1p controls acquisition of sodium tolerance is different from that mediating glucose regulation. *Microbiol. Sgm* **154**, 2814-2826. doi:10.1099/mic.0.2008/020149-0

Zyrina, A. N., Sorokin, M. I., Sokolov, S. S., Knorre, D. A. and Severin, F. F. (2015). Mitochondrial retrograde signaling inhibits the survival during prolong S/G2 arrest in *Saccharomyces cerevisiae*. *Oncotarget* **6**, 44084-44094. doi:10.18632/oncotarget.6406

Fig. S1

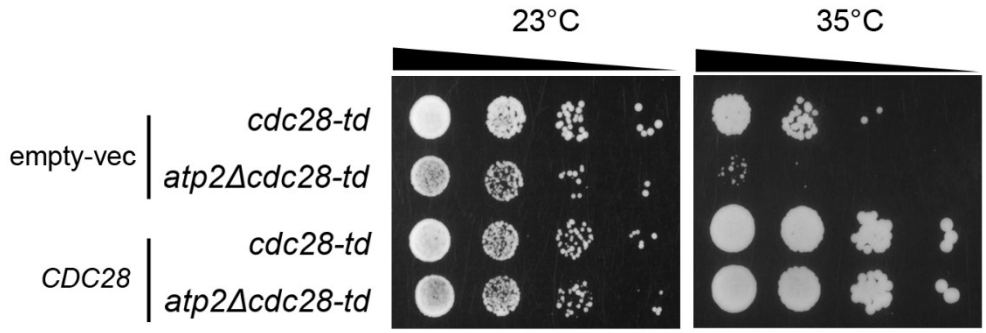

Fig. S1. Reintroducing wt Cdc28 restored the *atp2Δcdc28td* mutant growth at semi-permissive temperature. Growth analysis of *cdc28td* and *atp2Δcdc28td* transformed with empty-vector (YCP50) or the YCP50-derived pHLP183 vector (expressing *CDC28* from its natural promoter; a gift from Mark C. Hall (Hall, Jeong et al., 2008)). Cells were spotted in serial dilutions and grown at indicated semi-permissive temperatures. A representative result is shown (n=3).

Fig. S2

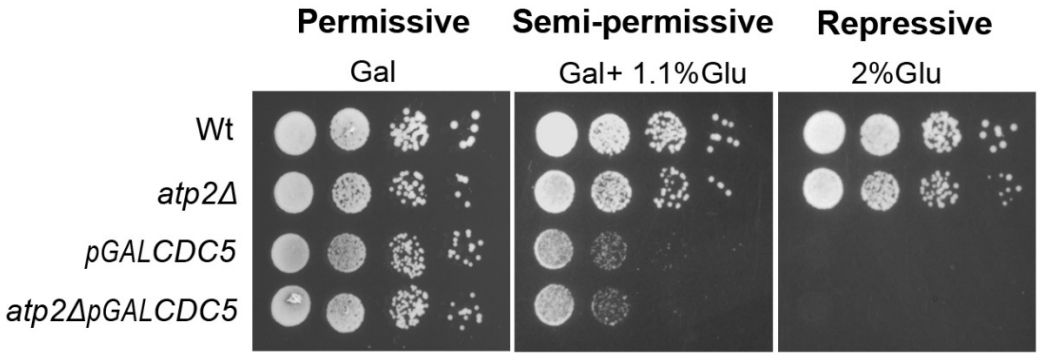

Fig. S2. *ATP2* does not genetically interact with the polo-like kinase encoding gene *CDC5*. Growth analysis of wt, *atp2*Δ, *pGAL1-CDC5* and *atp2*Δ*pGAL1-CDC5* strains. *CDC5* was placed under the control of *GAL1* promoter and partially or completely downregulated by growing the cells in the presence of the indicated concentrations of glucose. *CDC5* was placed under the control of the *GAL1* promoter by integrating the plasmid pFA6a-KanMX6-PGAL1-3HA into the wt and *atp2*Δ genomes upstream of *CDC5* (Longtine, McKenzie et al., 1998). Cells were spotted in fourfold serial dilutions. A representative image is shown (n=3).

Fig. S3

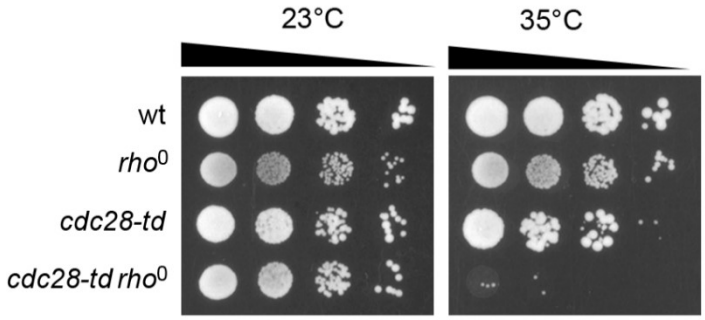

Fig. S3. Ablating mitochondrial DNA in a strain carrying the *cdc28-td* allele aggravates defective growth at semi-permissive temperature. Growth analysis of wt, rho^0, *cdc28td* and rho^0*cdc28td* spotted in serial dilutions and grown at permissive and semi-permissive temperatures. A representative result is shown (n=3). To generate *rho0* strains, cells were grown to saturation twice in liquid YPD medium plus ethidium bromide (25 µg/ml). Individual colonies were selected for growth defects on YPG plates and loss of mtDNA was confirmed by 4′,6-diamidino-2-phenylindole (DAPI) staining.

Fig. S4

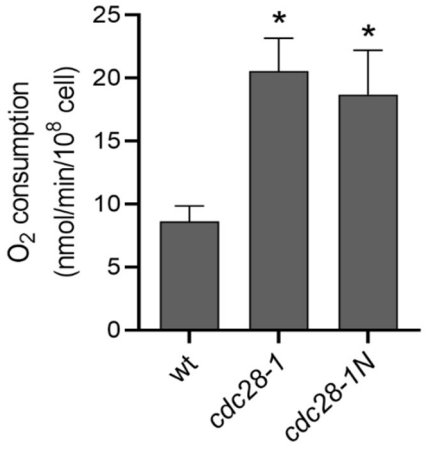

Fig. S4. Respiratory rate is increased in *cdc28-1* and *cdc28-1N* mutants at restrictive temperature. The basal respiratory rate was determined by measuring oxygen consumption in whole cells from glucose grown mid-log phase cultures at the restrictive temperature. Values are the mean ± SD (n =4); *, $p < 0.05$; one-way ANOVA.

Fig. S5

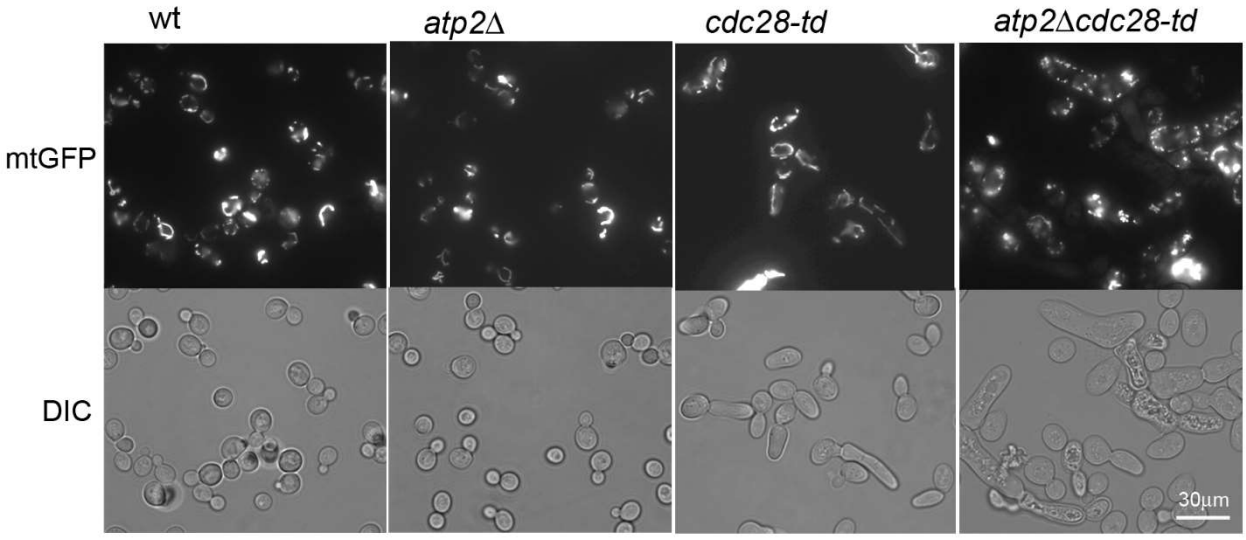

Fig. S5. Mitochondrial morphology is disrupted in double *atp2Δcdc28-td* strain. (A) Indicated yeast cells expressing mtGFP were analyzed by fluorescence microscopy. Representative images are DIC merged with maximum intensity projections of z stacks. Images were acquired by epifluorescence in a Zeiss Axio Imager Z1 microscope fitted with Nomarski optics with an Axiocam MR3.0 camera and Axiovision 4.7 software.

Fig. S6

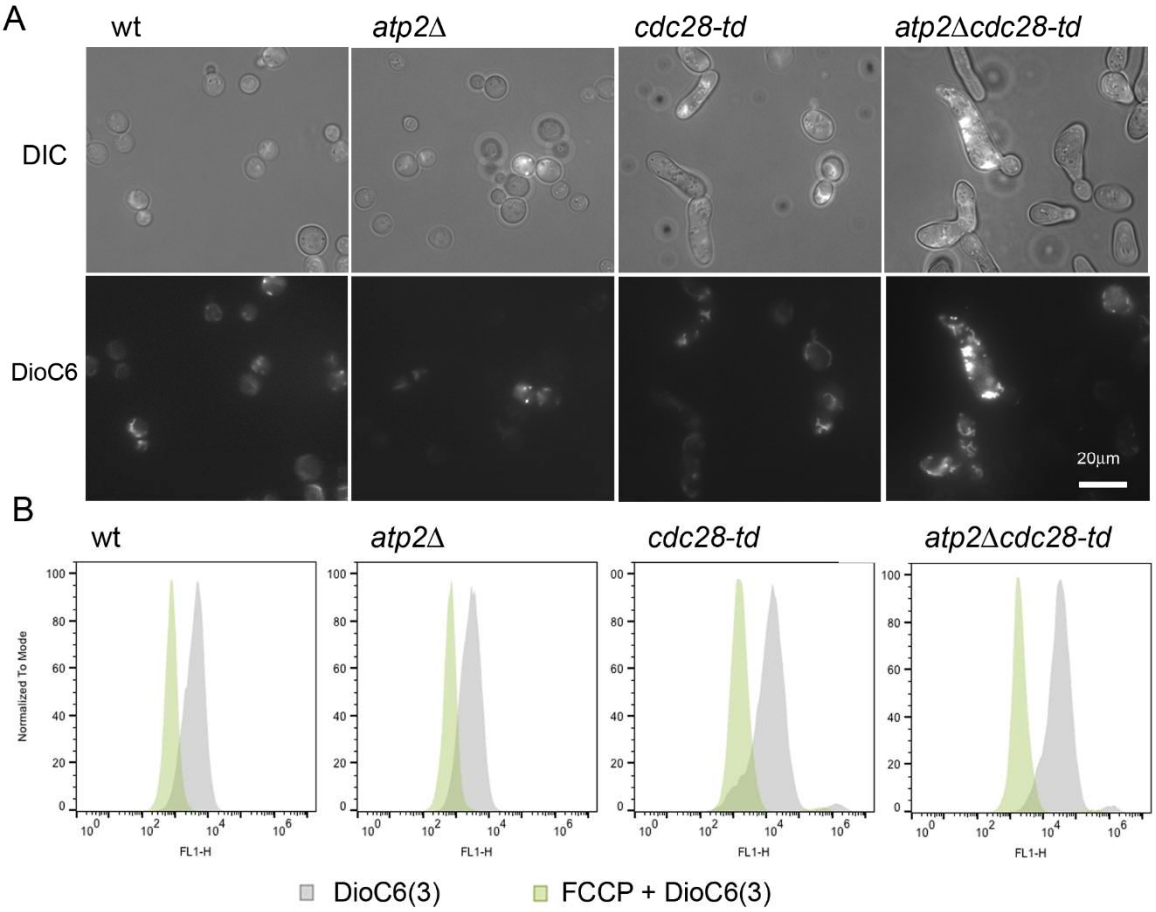

Fig. S6. Mitochondrial membrane potential is altered in double *atp2Δcdc28-td* mutant. (A) The mitochondrial localization of the fluorochrome DioC6(3) was checked by fluorescence microscopy. Representative images are DIC merged with maximum intensity projections of z stacks of DioC6(3) staining. (B) Addition of the FCCP protonophor, which dissipates the $\Delta\psi m$, lead to a substantial reduction of the $DiOC_6$ uptake for all strains.

Fig. S7

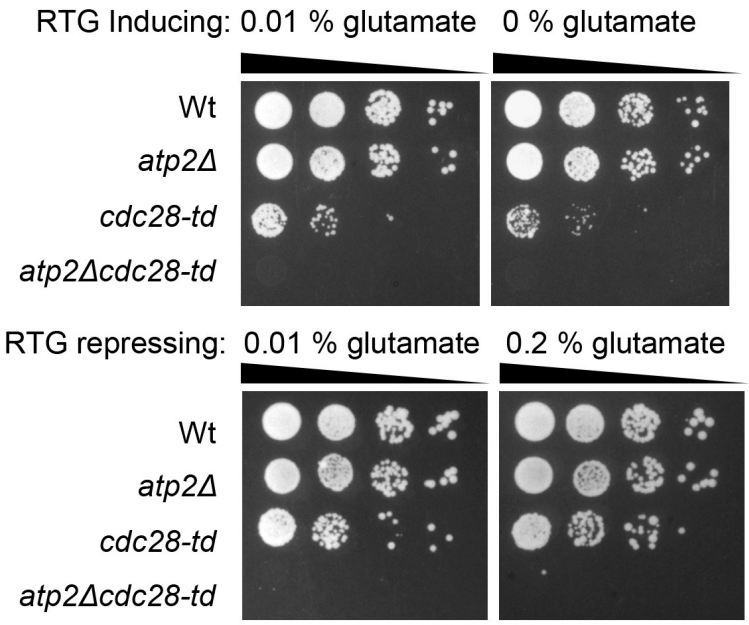

Fig. S7. Absence or excess of glutamate, a repressor of RTG-dependent gene expression, do not supress the growth defects of the *atp2Δcdc28-td* strain. Serial dilutions of indicated strains after growth at the semi-permissive temperature (35 ºC) in minimal media containing 0.01% glutamate (control), lacking or containing 0.2% glutamate.

Fig. S8

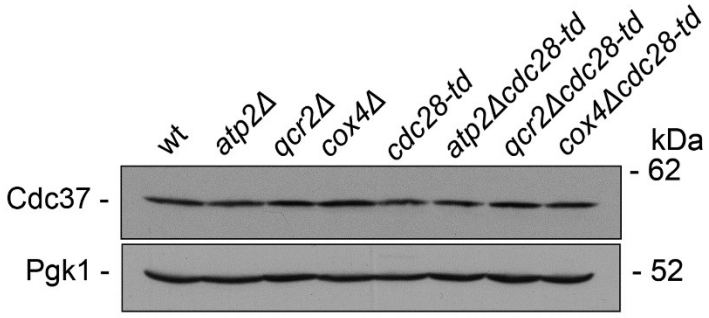

Fig. S8. Cdc37 levels are unchanged in OXPHOS mutants, single or in combination with *cdc28-td*. Western blot analysis of Cdc37 steady-state protein levels in indicated strains cultures at semi-permissive temperature of 26 ºC. Pgk1 is shown as loading control. A representative blot is shown (n=2).

Fig. S9

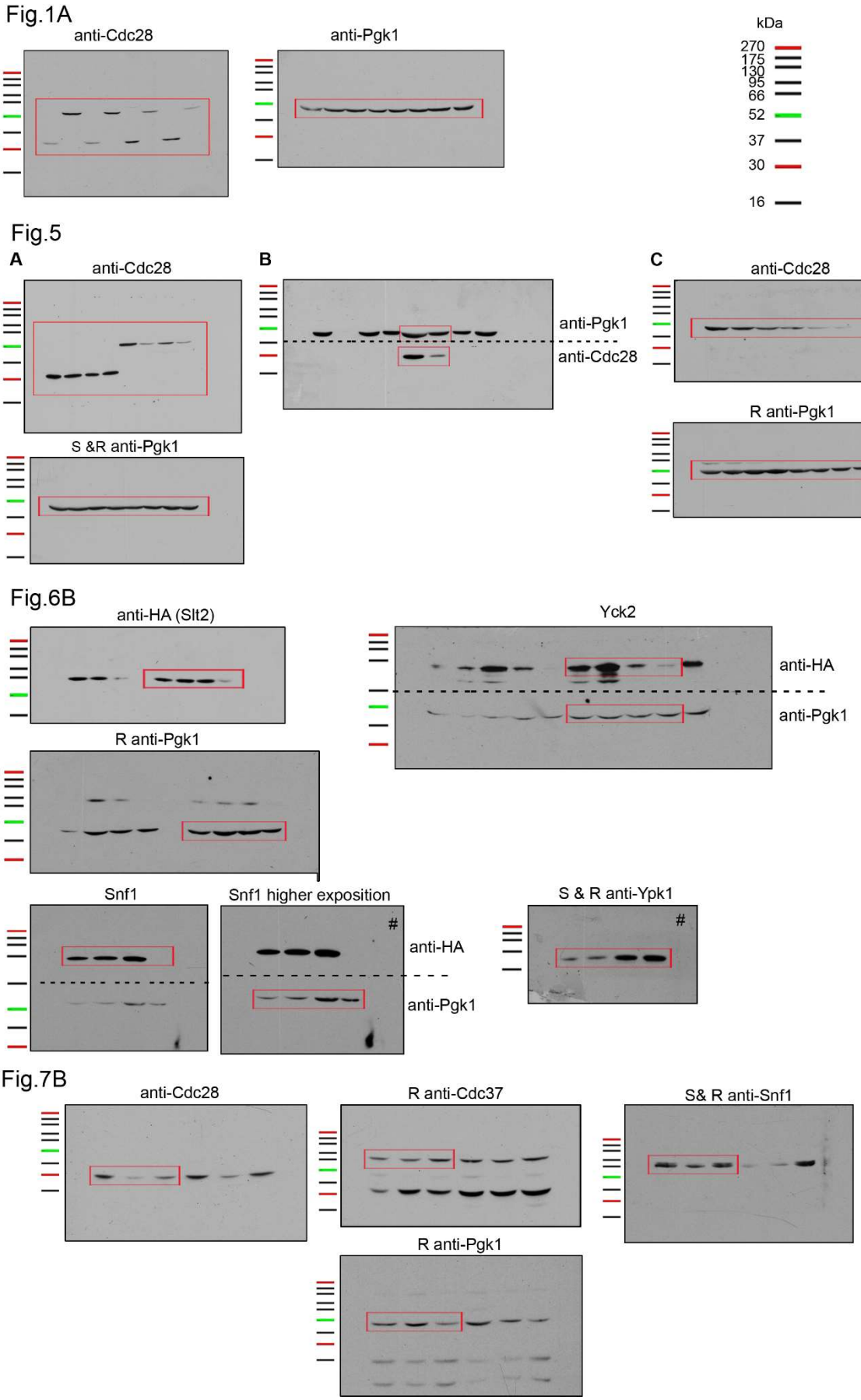

Fig. S9. Blot transparency. Full-length western blots with indicated antibodies and molecular weight markers are shown for bands displayed in Figures 1, 5-7. Protein Ladder: GRS Protein Marker MultiColour PLUS. Red rectangles are used to highlight where the bands were taken from. R indicates Reprobing; S & R indicates Stripping before Reprobing. Dotted line indicates where the membranes were cut for antibody incubation and re-aligned for imaging.

References

Hall MC, Jeong DE, Henderson JT, Choi E, Bremmer SC, Iliuk AB, Charbonneau H (2008) Cdc28 and Cdc14 control stability of the anaphase-promoting complex inhibitor Acm1. *J Biol Chem* 283: 10396-407

Longtine MS, McKenzie A, 3rd, Demarini DJ, Shah NG, Wach A, Brachat A, Philippsen P, Pringle JR (1998) Additional modules for versatile and economical PCR-based gene deletion and modification in Saccharomyces cerevisiae. *Yeast* 14: 953-61

Table S1. *S. cerevisiae* strains used in this study.

Strain	Genotype	Source
BY4741	Mat *a*; *his3Δ1 leu2Δ0 met15Δ0 ura3Δ0*	EUROSCARF
atp2Δ	BY4741; *atp2Δ::HIS3MX6*	Lab collection
cdc28-td	BY4741; *cdc28-td:KanMX4*	EUROSCARF [1]
atp2Δcdc28-td	BY4741; *atp2Δ::HIS3MX6 cdc28-td:KanMX4*	This study
cdc28-1	BY4741; *cdc28-1:KanMX4*	EUROSCARF [1]
atp2Δcdc28-1	BY4741; *atp2Δ::HIS3MX6 cdc28-1:KanMX4*	This study
cdc28-4	BY4741; *cdc28-4:KanMX4*	EUROSCARF [1]
atp2Δcdc28-4	BY4741; *atp2Δ::HIS3MX6 cdc28-4:KanMX4*	This study
cdc28-1N	BY4741; *cdc28-1N:KanMX4*	This study
atp2Δcdc28-1N	BY4741; *atp2Δ::HIS3MX6 cdc28-1N:KanMX4*	This study
cox4Δ	BY4741; *cox4Δ::HIS3MX6*	This study
cox4Δcdc28-td	BY4741; *cox4Δ::HIS3MX6 cdc28-td:KanMX4*	This study
qcr2Δ	BY4741; *qcr2Δ::HIS3MX6*	This study
qcr2Δcdc28-td	BY4741; *qcr2Δ::HIS3MX6 cdc28-td:KanMX4*	This study
atp1Δ	BY4741; *atp1Δ::HIS3MX6*	This study
atp1Δcdc28-td	BY4741; *atp1Δ::HIS3MX6 cdc28-td:KanMX4*	This study
atp4Δ	BY4741; *atp4Δ::HIS3MX6*	This study
atp4Δcdc28-td	BY4741; *atp4Δ::HIS3MX6 cdc28-td:KanMX4*	This study
rtg3Δ	BY4741; *rtg3Δ::URA3MX6*	This study
atp2Δrtg3Δcdc28-td	BY4741; *atp2Δ::HIS3MX rtg3Δ::URA3MX6 cdc28-td:KanMX4*	This study
cdc20-1	BY4741; *cdc20-1:KanMX4*	EUROSCARF [1]
atp2Δcdc20-1	BY4741; *atp2Δ::HIS3MX6 cdc20-1:KanMX4*	This study
ipl1-1	BY4741; *ipl1-1:KanMX4*	EUROSCARF [1]
atp2Δ ipl1-1	BY4741; *atp2Δ::HIS3MX6 ipl1-1:KanMX4*	This study
rho^0 *CIT2-LacZ*	BY4741; rho^0 *CIT2-LacZ:CIT2*	This study
CIT2-LacZ	BY4741; *CIT2-LacZ:CIT2*	This study
cdc28-td CIT2-LacZ	BY4741; *cdc28-td; CIT2-LacZ:CIT2*	This study
atp2Δcdc28-td CIT2-LacZ	BY4741; *atp2Δcdc28-td*; *CIT2-LacZ:CIT2*	This study
cdc28-1 CIT2-LacZ	BY4741; *cdc28-1; CIT2-LacZ:CIT2*	This study
atp2Δcdc28-1 CIT2-LacZ	BY4741; *atp2Δcdc28-1*; *CIT2-LacZ:CIT2*	This study
cdc28-1N CIT2-LacZ	BY4741; *cdc28-1N; CIT2-LacZ:CIT2*	This study
atp2Δcdc28-1N CIT2-LacZ	BY4741; *atp2Δcdc28-1N*; *CIT2-LacZ:CIT2*	This study
DH211	TM141 *cdc37Δ::HIS3* [Ycplac111 CDC37-HA]	[2]
DH212	TM141 *cdc37Δ::HIS3* [Ycplac111 cdc37-S14A-HA]	[2]

References

[1] Li, Z.J., et al., Nature Biotechnology, 2011. **29**(4): p. 361-U105.
[2] Hawle, P., et al.. Eukaryotic Cell, 2007. **6**(3): p. 521-532.